Signal Extraction in a Power-Recycled Michelson Interferometer with Fabry-Perot Arm Cavities Using a Multiple-carrier Frontal Modulation Scheme

Daniel Sigg[1], Nergis Mavalvala[2], Joseph Giaime[3], Peter Fritschel and David Shoemaker

LIGO Project
Department of Physics and Center for Space Research,
Massachusetts Institute of Technology, Cambridge, MA 02139

Accepted for publication in Applied Optics
May 1998

We present a signal extraction scheme for longitudinal sensing and control of an interferometric gravitational wave detector based on a multiple-frequency heterodyne detection technique. Gravitational wave detectors use multiple-mirror resonant optical systems where resonance conditions must be satisfied for multiple degrees of freedom that are optically coupled. The multiple-carrier longitudinal sensing technique provides sensitive signals for all interferometric lengths to be controlled and successfully decouples them. The feasibility of the technique is demonstrated on a table-top scale power-recycled Michelson interferometer with Fabry-Perot arm cavities and the experimentally measured values of the length sensing signals are in good agreement with theoretical calculations.

KEYWORDS

Gravitational-wave observatories, laser interferometer, modulation techniques, subcarrier, LIGO.

1. Present address: LIGO Project, P.O. Box 1970 S9-02, Richland WA 99352
Phone: (509) 372-8336; Fax: (509) 372-2178; E-mail: sigg_d@ligo.mit.edu.
2. Present address: LIGO Project, California Institute of Technology, MS 18-34, Pasadena CA 91125
Phone: (626) 395-3130; Fax: (626) 304-9834; E-mail: nergis@ligo.caltech.edu.
3. Present address: JILA CB 440, University of Colorado, Boulder C0 80309
E-mail: giaime@jila02.colorado.edu.

1 INTRODUCTION

Einstein's theory of general relativity predicts that gravitational-waves are ripples in the curvature of spacetime, radiated by accelerating aspherical mass distributions. The gravitational-wave induced spacetime distortion — or gravitational wave strain — stretches the space along one transverse axis and shrinks it along an orthogonal axis. Astrophysical sources are believed to be the most likely emitters of detectable gravitational radiation and since all known forms of matter are nearly transparent to gravitational waves, detection of gravitational waves holds the promise for a new and hitherto unexplored window into the universe. Gravitational radiation from the most promising astrophysical sources, such as coalescing neutron star or black hole binaries, is expected to produce strains of order 10^{-21} (in dimensionless units of change in length per unit length) [1]. Consequently, highly sensitive long baseline laser interferometers (LIGO [2], VIRGO [3], GEO600 [4] and TAMA300 [5]) are currently under construction with the objective of direct detection of gravitational radiation early in the next millennium.

The principle of interferometric detection of gravitational waves is based on measuring the optical phase shift due to path length changes induced by a passing gravitational wave [6]. For maximal strain sensitivity, the goal is to convert gravitational wave strain into optical phase as efficiently as possible. The detectors currently planned for the Laser Interferometer Gravitational-wave Observatory (LIGO) [7] are variants of a simple Michelson interferometer (see Fig. 1). A 4 kilometer long resonant Fabry-Perot cavity in each arm of the Michelson interferometer stores the laser light for a time of the order of the gravitational wave period at 100 Hz, thus increasing the phase sensitivity by the number of times the photons traverse the cavity. To reduce sensitivity to fluctuations in power of the incident laser light, the antisymmetric or signal extraction port of the Michelson interferometer is held on a dark fringe, resulting in almost all the light returning towards the laser. A partially transmitting mirror is placed between the laser and the beam splitter. When located at the correct longitudinal position, this power-recycling mirror (RM) reflects most of the light back toward the beam splitter (BS), that is, the light is recycled. The consequent increase in effective incident power — by a factor known as the power-recycling gain — enhances the gravitational wave strain sensitivity [8],[9],[10]. The power-recycling cavity is formed by the recycling mirror as the input coupler and the symmetric port of the Michelson interferometer (comprised of the beam splitter and the two input test masses) which serves as a complex end "mirror".

This optical configuration has four length degrees of freedom which must be controlled to hold the interferometer mirrors at positions where the resonance conditions for optimal sensitivity are satisfied. The lengths of the two Fabry-Perot arm cavities, L_1 and L_2, must be held on resonance, as must the average length of the power-recycling cavity, $l_C = (l_1 + l_2)/2$. The path length difference in the arms of the Michelson interferometer, $l_D = (l_1 - l_2)/2$, must be controlled to maintain the dark fringe condition. All four lengths must be controlled to within a tiny fraction of a wavelength.

An elegant method to hold the interferometer's common-mode degrees-of-freedom ($l_C = (l_1 + l_2)/2$ and $L_C = (L_1 + L_2)/2$) on resonance is a variant of the reflection sensing technique [11],[12], where phase modulation sidebands at radio frequencies (RF) are imposed on the input light and a heterodyne detection scheme is used to measure the deviations from resonance. The carrier field reflected from the resonant cavity interferes with the non-resonant

sideband field (which acts as a constant-phase reference), giving an RF intensity signal that is proportional to the deviation from resonance.

To sense the differential degrees of freedom in a Michelson interferometer, L. Schnupp proposed the use of a macroscopic length asymmetry to couple frontal phase modulation sidebands out the antisymmetric port [13]. This asymmetry shifts the sidebands away from the dark fringe, allowing the use of a suppressed carrier detection scheme at the antisymmetric port (see Fig. 1) to sense the deviation from a dark fringe for the carrier.

A scheme to control all longitudinal degrees of freedom with just one pair of sidebands, that is, with a *single carrier* frontal modulation scheme has been demonstrated using a gain hierarchy implemented in the servo control to separate the power-recycling cavity length from the common arm cavity length [14]. This work presents a *multiple-carrier* frontal modulation scheme [15] with asymmetry readout [16]. An additional carrier — the so-called subcarrier, which is not resonant in the arm cavities — is used with its own set of RF sidebands to probe the two degrees of freedom associated with the power-recycled Michelson interferometer. The response of the sensor signals to deviations of the interferometer lengths is best represented as a matrix, referred to as the length sensing matrix. The implementation of the control system is greatly simplified if the length sensing matrix is diagonal and robust against small changes in the optical parameters of the interferometer. This is indeed achieved with the multiple-carrier frontal modulation scheme since the subcarrier separates the Michelson degrees of freedom from the arm cavity lengths. This scheme has the advantage of yielding Michelson error signals that are less sensitive to the resonant state of the arm cavities. In fact, if the lengths are expressed as common-mode and differential deviations, the length sensing matrix becomes nearly diagonal.

2 THEORY AND DESIGN

In a power-recycled Michelson with cavities in the arms the carrier (C) is resonant in all three cavities. Since the beam splitter naturally separates common-mode and differential fields, the reflection port of the interferometer resembles a linear system of coupled cavities (three mirrors in series) for common-mode arm cavity variations. A pair of sidebands which are resonant in the power-recycling cavity are imposed on the carrier light incident on the interferometer. The sidebands are not resonant in the arm cavities so the field returning from the beam splitter can be used to extract a signal which is highly sensitive to common-mode length deviations of the arm cavities. Since the carrier sidebands (CSB) are resonant in the power-recycling cavity but do not produce a dark fringe at the antisymmetric port, substantial sideband power is transmitted to the antisymmetric port, leading to a signal which is sensitive to differential arm cavity length deviations.

Writing the free spectral range of the power-recycling cavity as $2f_0$, where

$$f_0 = \frac{c}{4l_C} \tag{1}$$

the fields that resonate in the power-recycling cavity only occur at frequency intervals of $2f_0$. Upon reflection from the resonant arm cavity, the carrier acquires a phase shift of π relative to the carrier sidebands, which are outside the arm cavity resonance. If all other frequencies are

referenced to the carrier double resonance then the carrier sidebands resonate at frequency intervals of $2f_0$, but shifted by f_0 relative to the carrier resonance, that is,

$$\Delta\nu_{CSB} \equiv f_{CSB} = \pm(2m+1)f_0 \tag{2}$$

where m is an integer and $m = 0$ for the carrier double resonance.

For a system that is optimized for gravitational wave sensitivity, almost no carrier power is reflected from the interferometer. This is achieved by choosing the power transmissivity of the power-recycling mirror to be approximately equal to the total loss in the Michelson interferometer with arm cavities, that is, the carrier is critically matched [17]. The transmission of the carrier sidebands out the anti-symmetric port is determined by the macroscopic Michelson path length asymmetry, l_D. The most efficient transfer of sideband power to the antisymmetric port is achieved by making the fraction of the carrier sideband power directed out the antisymmetric port due to the asymmetry equal to the power-recycling mirror power transmissivity, that is,

$$T_{RM} \approx \sin^2\left(\frac{4\pi f_{CSB}}{c} l_D\right) \tag{3}$$

Of course, if the carrier sidebands are also critically matched via the asymmetry losses, then negligible carrier sideband field is reflected from the interferometer and the carrier double resonance signal must be extracted from the fields inside the power-recycling cavity.

The role of the subcarrier (SC) and its sidebands is to detect deviations in the power-recycled Michelson lengths (the signals from the carrier and carrier sidebands sense the arm cavity length deviations). To ensure that the subcarrier frequency family is insensitive to the arm cavity lengths, we choose the frequency of the subcarrier to be exactly anti-resonant in the arm cavity, that is,

$$f_{SC} = \left(n + \frac{1}{2}\right) FSR_{ARM} = \left(n + \frac{1}{2}\right) \frac{c}{L_1 + L_2} \tag{4}$$

where n is an integer and FSR_{ARM} refers to the average free spectral range of the arm cavities. We expect a relative phase shift of π between carrier and subcarrier due to anti-resonance in the arm cavity. However, the subcarrier can be adjusted to experience a phase shift of π due to the asymmetry. The amplitude reflection coefficient of the field retro-reflected from the Michelson interferometer with arm cavities is given by

$$r_M \propto \cos\left(\frac{4\pi f}{c} l_D\right) \tag{5}$$

The reflection coefficient of the Michelson, r_M, varies sinusoidally as a function of frequency for a fixed asymmetry, l_D. Light at the frequency for which $r_M = -1$ effectively undergoes a phase shift of π. In most practical cases, the carrier phase is shifted by π due to resonance in the arm cavity, while the subcarrier acquires a phase shift of π due to the asymmetry, and there is hence no relative phase shift between them. In the power-recycling cavity, for light at frequencies such that $r_M < 0$, resonance occurs at even multiples of f_0. Consequently, the frequency of the subcarrier relative to the carrier is given by

$$\Delta\nu_{SC} \equiv f_{SC} = 2pf_0 \tag{6}$$

and phase modulation sidebands imposed on the subcarrier (SCSB), which are to be resonant in the power-recycling cavity, must obey

$$\Delta\nu_{SCSB} \equiv f_{SC} - f_{SCSB} = \pm 2q f_0 \tag{7}$$

where p and q are integers. Using the suppressed carrier scheme based on the subcarrier and subcarrier resonant sidebands at the antisymmetric port will give an error signal which holds the subcarrier on the dark fringe. To simultaneously satisfy the dark fringe condition for the carrier, the wavelength associated with the subcarrier frequency shift must be an exact multiple of twice the asymmetry, for example,

$$\frac{c}{f_{SC}} = 2l_D \tag{8}$$

Moreover, this choice minimizes the shot noise at the antisymmetric port, since destructive interference of the carrier and subcarrier fields ensures minimal power leaking out at this port.

In principle, the power-recycling cavity length could be sensed using the signal from the subcarrier and its resonant sidebands, SCSB, at either the reflection port or by picking off a tiny fraction of the field inside the power-recycling cavity. This is possible because, despite the fact that both are resonant in the power-recycling cavity, the asymmetry losses guarantee a different phase sensitivity for the subcarrier and its resonant sidebands. The signal strength is, however, strongly dependent on the relative losses for the subcarrier and the resonant sidebands in the power-recycling cavity and a more robust solution is to add an additional pair of sidebands to the subcarrier, that are not resonant in any cavity. These non-resonant sidebands, the SCNR, do not couple into the interferometer at all and are chosen to have a minimal overlap with both longitudinal and transverse modes of the power-recycling cavity to ensure low coupling into the interferometer.

In Fig. 2 we plot the amplitude of the fields inside the power-recycling cavity (a) and at the antisymmetric port (b) as a function of frequency. The horizontal axis is in terms of the dimensionless quantity f/f_0. The carrier resonance occurs at $f/f_0 = 0$, the carrier sidebands at $f = (\pm 1, \pm 3, \pm 5) f_0$, the subcarrier at $f = 20 f_0$, and the subcarrier resonant sidebands at $f = (20 \pm 2, 20 \pm 4) f_0$. The subcarrier non-resonant sidebands are ideally in the valleys, at $f = (20 \pm 1, 20 \pm 3) f_0$, so that they do no couple into the interferometer.

The mirror radii of curvature, along with the cavity lengths, influence the characteristics of the fundamental gaussian mode and the transverse mode spacing of the cavity. To ensure that none of the circulating frequencies excite higher-order transverse modes in the cavity, coincidences in the frequencies of the higher-order modes with the modulation frequencies are avoided. The lengths of the cavities directly influence the allowed modulation frequencies, and the multiple resonance/anti-resonance conditions determine their relative lengths. By varying the mirror radii of curvature (while maintaining compatibility of the fundamental mode in the arm and power-recycling cavities) we can achieve optimum mode spacing for avoidance of the higher-order transverse modes.

Mirror reflectivities are chosen to optimize the interferometer sensitivity to gravitational-waves. With arm cavity end mirror reflectivities as close to unity as possible, the arm cavity input mirror reflectivities are chosen to give a storage time comparable to the lowest frequency gravitational

wave of interest; the power-recycling mirror reflectivity is chosen for near-critical matching of the carrier, for given interferometer losses.

The technical limitations of radio frequency techniques and the physical constraints on the interferometer parameters combine to determine the choice of modulation parameters. Phase-modulation frequencies above 5 MHz are used to ensure that the laser technical intensity noise does not dominate over shot noise. On the other hand, working at frequencies below 100 MHz makes the implementation of the electronics more practical. For the carrier sidebands to efficiently exit the antisymmetric port, modulation frequencies of tens of megahertz are necessary given the practical asymmetry of few tens of centimeters. Consequently, the subcarrier frequency shift must be a few hundred megahertz to ensure the dark port condition for both the carrier and subcarrier.

3 Experimental Verification

We define the length sensing matrix L such that

$$S_i(t, \delta l) = 2J_0(\Gamma_i)J_1(\Gamma_i)P_i\sum_j L_{ij}\delta l_j \cos(\Omega_i t + \phi_{ij}) \tag{9}$$

where S_i is the light intensity at the modulation frequency on the i-th sensor; δl_j is the deviation from resonance of the j-th degree of freedom; L_{ij} are the elements of the length sensitivity matrix in the static field limit; ϕ_{ij} is an intrinsic RF phase; P_i is the power on the i-th detector; Ω_i and Γ_i are the RF modulation frequency and depth, respectively, for the i-th sensor.

A table-top scale interferometer was constructed to test this multiple carrier scheme by quantitative determination of the length sensitivity matrix, L. A schematic overview of the table-top scale Fixed Mirror Interferometer experiment is shown in Fig. 3. The laser source is a frequency and power stabilized CW Ar^+ laser with a wavelength of 514.5 nm and typical output power of 250 mW. The laser light is split into two paths; the light transmitted through BS1 is used for the frequency stabilization and the reflected light goes to the main interferometer input optics train. Light reflected from BS1 is further split by BS2. The reflected beam is the carrier path where PC3 generates the carrier sidebands; the transmitted light is used to generate the frequency-shifted subcarrier. Vertically polarized light reflected from PBS2 passes through an acousto-optic modulator (AOM) modulated at 195.5 MHz and a curved mirror reflects the frequency shifted component back toward the AOM. The light which passes twice through the AOM acquires a frequency shift of 391 MHz with respect to the carrier. Double passing the quarter-wave plate (QWP) converts vertically polarized light to horizontally polarized so the 391 MHz component is transmitted through PBS2. PC4 and PC5 impress the subcarrier resonant and non-resonant phase modulation sidebands, respectively. Carrier and subcarrier light with all the associated modulation frequencies are recombined on BS3 and launched into a fiber which serves as a spatial mode filter.

Wherever possible, optical design choices were made which minimize differences from the LIGO-scale application and which allow the significant features of the scheme to be verified. The arm cavities have a finesse of $F \approx 160$. The power-recycling mirror transmissivity is a few percent greater than the total interferometer losses to allow for possible degradation of mirror quality or loss accumulation. A pellicle pick-off in the power-recycling cavity and imperfect contrast at the beam splitter introduce an additional loss of 5% in the power-recycling cavity,

leading to a power-recycling gain of ~7 for the main carrier. The interferometer parameters are listed in Table 1.

The fields at the reflection port are detected using the rejected beam from a Faraday isolator (FI); a pellicle (RCPO) picks off ~1% of the light inside the power-recycling cavity. Light from these two ports and from the dark port is incident on five RF-tuned photodetectors, demodulated at their respective modulation frequencies, and the resulting error signals are used to servo-control the length degrees of freedom of the interferometer. The carrier and carrier sideband signal in reflection (PD2) is redundant with the corresponding signal at the RCPO (PD3); it is used mainly as a consistency check.

The photodetectors are comprised of photodiodes followed by a tuned circuit, an RF amplifier, and a mixer with low-pass filtering to achieve a low noise down-conversion of the length error signal at the modulation frequency. These error signals are fed back to piezo-electric transducers (PZTs) controlling the axial position of the interferometer mirrors. Each longitudinal degree-of-freedom is controlled by two PZT actuators: one with a small bandwidth (~100 Hz), but a large dynamic range (~2 μm) and the other with a small dynamic range (~0.2 μm), but a large bandwidth (~20 kHz). Since the interferometer is operated in air with minimal seismic or acoustic isolation, high bandwidth and large dynamic range are crucial for a reliable length lock.

To measure the length sensitivity matrix a modulation signal is added to one of the error signals of the length servo. The optical response is then deduced from the ratio of the measured error signal (photodiode) over the measured control signal (PZT), that is, the forward gain of optical plant. This measurement is repeated for each longitudinal degree-of-freedom. The signals are digitized by analog-to-digital converters under control of a VME-based computer system. Since the control signals at low frequencies are dominated by acoustic and seismic noise, a modulation frequency of 2.2 kHz is chosen. Unfortunately, the highest sampling rate achievable by our system is only 1 kHz. To make a meaningful measurement the signals are first high-pass filtered to remove the low frequency component, before they are undersampled. As a result the 2.2 kHz modulation frequency is aliased down to 200 Hz. Since angular alignment can reduce the power build-up in a cavity and, therefore, lower the length sensitivity, an auto-alignment system [18],[19] is turned on prior to each measurement. This stabilizes each mirror angle to within 1% of the divergence angle (that is, 1% of 0.24 mrad or 2.4 μrad). In our case, the quadrant photodiodes of the alignment system — which are placed exactly at the same ports as the length sensors — have the advantage that their response was previously calibrated in absolute values. Consequently, the sum of all four quadrants is used for the measurement of the error signal, rather than the signals coming from the monolithic length photodiodes.

The amplitude spectral densities of the measured time series for each sensor are computed using off-line analysis tools. The actuator signal amplitude at 2.2 kHz is used to determine the displacement modulation applied to each degree of freedom. Normalizing the sensor signals to the input light power, modulation depths, the quantum efficiency and the transimpedance of the sensors, the length sensitivity matrix of the interferometer is calculated.

Since the free spectral range of a cavity is well known from its length, the response of the PZT actuators can be calibrated by driving through multiple resonances of (sub)carrier and sidebands. The calibration errors of the length actuators were then estimated to be about 10%. The uncertainty of the light built-up in the power-recycling cavity is estimated from the knowledge of the total power losses. An uncertainty of 0.01 in the round-trip loss of the power-recycling cavity

will affect the length sensitivities by 16% – 25%, depending on the matrix element. The estimated errors from the transimpedance gains of the photodetectors are 5% for modulation frequencies below 40 MHz and 10% otherwise. The uncertainties of the photodetector quantum efficiency and the absolute light power incident on each detector give additional errors of 5% and 6%, respectively. The statistical errors are estimated from the noise level in the measured power spectrums. For diagonal elements the statistical errors are between 1% and 6%. Since off-diagonal elements are generally small, their measured values can easily be dominated by statistical fluctuations. Since the above errors are independent of each other they are added in quadrature.

4 Results

The matrix elements are predicted using a plane wave model of the interferometer (equivalent to a model with a single TEM_{00} mode) where the phase modulated fields are propagated and the sensitivity of the sensor signals to small deviations from resonance are calculated. The experimentally determined values for the matrix elements are compared with the model values in Table 2. Good agreement with the model is found, with the predicted values of most elements lying within experimental error bars. All measured matrix elements that dominate the rows of the sensitivity matrix are within 20% to 40% (28% on average) of the model prediction. (The other values are generally small and unimportant.) In addition, we find that the design philosophy of a highly non-singular — and therefore robust — control matrix has been realized and was observed experimentally to be advantageous. We conclude that the multiple-carrier frontal modulation scheme successfully decouples the sensing signals for the length degrees of freedom of a power-recycled Michelson interferometer with Fabry-Perot arm cavities.

The planned control topology for the initial LIGO interferometer is based on a single carrier frontal modulation scheme because of the relative simplicity of its optical implementation. However, possible future configurations — such as a Mach-Zehnder readout [20] or a dual recycled interferometer [21] — may not have “good” length discriminants for control of all degrees of freedom with a single carrier scheme only and, therefore, additional frequencies may be inevitable.

ACKNOWLEDGMENTS

We thank our colleagues on the LIGO project, in particular Rainer Weiss and Stan Whitcomb; their numerous useful suggestions and insightful comments helped us carry out this experiment. Our special thanks to Yaron Hefetz, with whom the experiment was initiated. This work is supported by NSF grant PHY-9210038. One of us (D. Sigg) was partially supported by the Swiss National Science Foundation.

REFERENCES

[1] See, for example, K. S. Thorne, "Gravitational radiation," in *300 Years of Gravitation*, S. W. Hawking and W. Israel, eds. (Cambridge University Press, Cambridge, 1987), 330–458.

[2] F. J. Raab, "The LIGO project: progress and prospects," in *First Edoardo Amaldi Conference on Gravitational Wave Experiments*, E. Coccia, G. Pixella and F. Ronga, eds. (World Scientific, Singapore, 1995), pp. 70–85.

[3] A. Giazotto, "The VIRGO experiment: status of the art," ibid., pp. 86–99.

[4] K. Danzmann, "GEO600 — A 600 m laser interferometric gravitational wave antenna," ibid., pp. 100–111.

[5] K. Tsubono, "300 m laser interferometric gravitational wave detector (TAMA300) in Japan," ibid., pp. 112–114.

[6] R. Weiss, "Electromagnetically coupled broadband gravitational antenna," MIT Res. Lab. Electron. Q. Prog. Rep. **105**, 54-76 (1972).

[7] A. Abramovici, W. E. Althouse, R. W. P. Drever, Y. Gürsel, S. Kawamura, F. J. Raab, D. Shoemaker, L. Sievers, R. E. Spero, K. S. Thorne, R. E. Vogt, R. Weiss, S. E. Whitcomb and M. E. Zucker, "LIGO: the Laser Interferometer Gravitational-wave Observatory," Science **256**, 325–333 (1992).

[8] R. W. P. Drever, J. Hough, A. J. Munley, S.-A. Lee, R. Spero, S. E. Whitcomb, H. Ward, G. M. Ford, M. Hereld, N. A. Robertson, I. Kerr, J. R. Pugh, G. P. Newton, B. Meers, E. D. Brook III, and Y. Gürsel, "Gravitational wave detectors using laser interferometers and optical cavities," in *Quantum Optics, Experimental Gravity and Measurement Theory*, P. Meystre and M. O. Scully, eds. (Plenum Press, New York, 1983) pp. 503—524.

[9] H. Billing, K. Maischberger, A. Rüdiger, R. Schilling, L. Schnupp and W. Winkler, "The Munich Gravitational Wave Detector Using Laser Interferometry," in *Quantum Optics, Experimental Gravity, and Measurement Theory*, P. Meystre and M. O. Scully, eds. (Plenum Press, New York, 1983) pp. 525-566.

[10] D. Schnier, J. Mizuno, G. Heinzel, H. Lück, A. Rüdiger, R. Schilling, M. Schrempel, W. Winkler and K. Danzmann, "Power recycling in the Garching 30 m prototype interferometer for gravitational-wave detection," Phys. Lett. A **225,** 210-216 (1997).

[11] A. Schenzle, R. DeVoe and G. Brewer, "Phase-modulation laser spectroscopy," Phys. Rev. A **25**, 2606–2621 (1982).

[12] R. W. P. Drever, J. L. Hall, F. V. Kowalski, J. Hough, G. M. Ford, A. J. Munley and H. Ward, "Laser phase and frequency stabilization using an optical resonator," Appl. Phys. B **31**, 97–105 (1983).

[13] L. Schnupp, Max-Planck-Institut für Quantenoptik, D-85748 Garching, Germany, private communication (1986).

[14] M. W. Regehr, F. J. Raab, and S. E. Whitcomb, "Demonstration of a power-recycled Michelson interferometer with Fabry-Perot arms by frontal modulation," Opt. Lett. **20**, 1507–1509 (1995).

[15] J. A. Giaime, "Studies of laser interferometric design and a vibration isolation system for interferometric gravitational wave detectors," Ph. D. dissertation (Massachusetts Institute of Technology, Cambridge, Mass., 1995).

[16] N. Mavalvala, "Alignment issues in laser interferometric gravitational-wave detectors," Ph. D. dissertation (Massachusetts Institute of Technology, Cambridge, Mass., 1997), p. 23.

[17] A. E. Siegman, *Lasers* (University Science, Calif., 1986), p. 423.

[18] Y. Hefetz, N. Mavalvala and D. Sigg, "Principles of calculating alignment signals in complex resonant optical interferometers," J. Opt. Soc. Am. B **14**, 1597–1605 (1997).

[19] N. Mavalvala, D. Sigg and D. Shoemaker, "Experimental test of an alignment sensing scheme for a gravitational-wave interferometer," submitted to Optics Letters (1998).

[20] C. N. Man, D. Shoemaker, M. Pham Tu and D. Dewey, "External modulation technique for sensitive interferometric detection of displacements," Phys. Lett. A **148**, 8-16 (1990).

[21] B. J. Meers, "Recycling in laser-interferometric gravitational-wave detectors," Phys. Rev D **38** 2317-2326 (1988).

FIGURE CAPTIONS

Figure 1: Optical layout of an interferometric gravitational wave detector to be used by LIGO. RM refers to the power recycling mirror, BS to the beam splitter, ITM to the input test mass and ETM to the end test mass.

Figure 2: Amplitude of the fields (relative to the input power) as a function of frequency offset from the double resonance of the carrier (in units of f_0, the half free spectral range of the power-recycling cavity) in (a) the power-recycling cavity and (b) at the antisymmetric port. The narrow carrier double resonance occurs at $f = 0$ and again at $f = \pm 13.3 f_0$, the free spectral range of the arm cavity. The field amplitude in the power-recycling cavity at $f = 0$ is lower than the one at $f = 20 f_0$ (the subcarrier resonance), since the carrier sees additional losses in the arm cavities. The sinusoidal envelop is due to the Michelson transmissivity corresponding to the asymmetry. The interferometer parameters used in this calculation are given in Table 1.

Figure 3: Schematic overview of the Fixed Mirror Interferometer, including the input optics train.

TABLES

Modulation frequencies	Interferometer lengths	Mirror radii of curvature	Mirror power reflectivities	Mirror power losses
f_{CSB} = 58.7 MHz f_{SC} = 391 MHz f_{SCSB} = 39.1 MHz f_{SCNR} = 32.3 MHz	l_C = 3.84 m $L_1 = L_2$ = 0.575 m l_D = 0.383 m	Rad_{RM} = 6.0 m $Rad_{ITM} = \infty$ Rad_{ETM} = 15.0 m	R_{RM} = 0.93 R_{BS} = 0.475 R_{ITM} = 0.97 R_{ETM} = 0.999885	L_{RM} = 0.005 L_{BS} = 0.050 $L_{ITM} = 50 \times 10^{-6}$ $L_{ETM} = 100 \times 10^{-6}$

Table 1: Interferometer parameters for the Fixed Mirror Interferometer experiment.

Sensor, rf-phase and photodetector	l_D		l_C		L_1		L_2	
	meas.	**calc.**	**meas.**	**calc.**	**meas.**	**calc.**	**meas.**	**calc.**
SCSB, Q-phase, PD5	**–40(10)**	**–43**	1.7(4)	0	2.1(25)	–0.24	–2.8(25)	–0.22
SCNR, I-phase, PD1	–06(20)	0.1	**200(50)**	**215**	28(30)	1.2	–31(30)	1.1
CSB, Q-phase, PD4	–54(35)	–40	–10(35)	0.05	**–2220(490)**	**–1940**	**1700(490)**	**1945**
CSB, I-phase, PD2	–120(90)	–5.7	60(90)	94	**3400(1100)**	**5144**	**4900(1100)**	**5146**
CSB, I-phase, PD3	–350(650)	205	270(650)	–346	**26000(11000)**	**36500**	**41000(11000)**	**36510**

Table 2: The measured values (with their experimental errors in parentheses) and the calculated values of the length sensitivity matrix. The most important values are shown in bold face. The photodetector positions are given in Fig. 3.

FIGURES

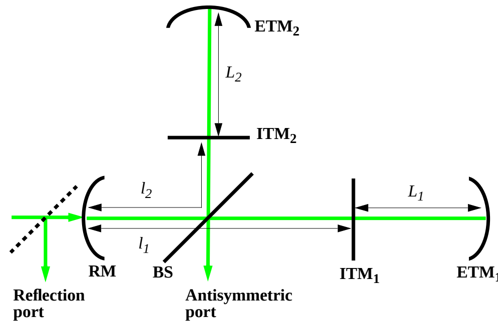

Figure 1 Sigg

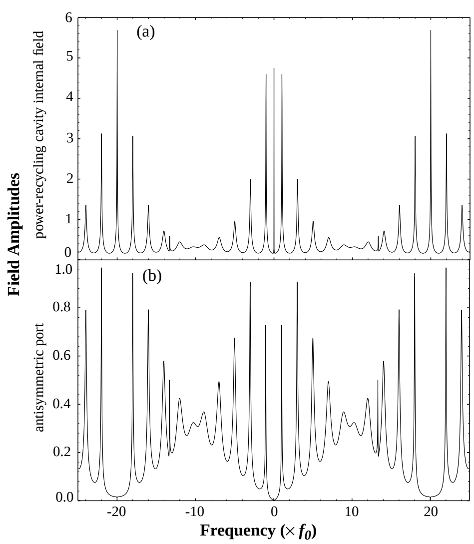

Figure 2 Sigg

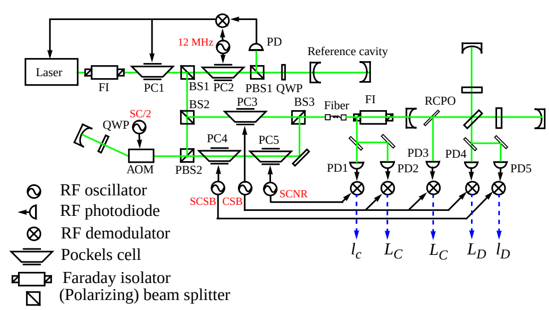

Figure 3 Sigg